THE JOURNAL OF PHYSICAL CHEMISTRY B

ARTICLE

pubs.acs.org/JPCB

Circular Dichroism and Ultraviolet Resonance Raman Indicate Little Arg-Glu Side Chain α-Helix Peptide Stabilization

Zhenmin Hong, Zeeshan Ahmed,[†] and Sanford A. Asher*

Department of Chemistry, University of Pittsburgh, Pennsylvania 15260, United States

Supporting Information

ABSTRACT: Electrostatic interactions between side chains can control the conformation and folding of peptides and proteins. We used circular dichroism (CD) and ultraviolet (UV) resonance Raman spectroscopy (UVRR) to examine the impact of side chain charge on the conformations of two 21 residue mainly polyala peptides with a few Arg and Glu residues. We expected that attractions between Arg-10 and Glu-14 side chains would stabilize the α-helix conformation compared to a peptide with an Arg-14. Surprisingly, CD suggests that the peptide with the Glu-14 is less helical. In contrast, the UVRR show that these two peptides have similar α-helix content. We conclude that the peptide with Glu-14 has the same net α-helix content as the peptide with the Arg but has two α-helices of shorter length. Thus, side chain interactions between Arg-10 and Glu-14 have a minor impact on α-helix stability. The thermal melting of these two peptides is similar. However the Glu-14 peptide pH induced melting forms type III turn structures that form α-helix-turn-α-helix conformations.

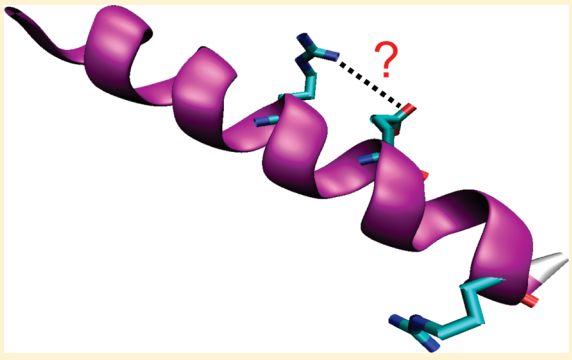

INTRODUCTION

For most proteins, the information needed to fold into their native states is encoded in their primary sequences.[1,2] Despite decades of studies of protein folding, it is still impossible to predict the secondary structure of a protein from only its primary sequence, if an analogous sequence has not been previously characterized. The native structure is determined by amino acid side chain interactions such as hydrophobic interactions, hydrogen bonding, and electrostatic interactions. The strength and long-range nature of electrostatic interactions allow them to dominate side chain interactions. Side chain ion pairs are commonly found in protein crystal structures, especially within the hydrophobic cores of protein.[3−7] However, the impact of these types of interactions on, for example, α-helix structures is still unclear.[8−24]

We have been using UV resonance Raman spectroscopy (UVRR) to examine equilibrium protein and peptide solution conformations, as well as the kinetics of unfolding.[25−37] We recently developed a method to determine the Gibbs free energy landscape along the Ramachandran Ψ angle folding coordinate.[37−39] We also monitored the kinetics of folding of α-helical peptides and were able to monitor both 3_{10} helix and π bulge conformations in equilibrium with the pure α-helix conformation.

In the work here, we use UVRR and CD to examine the solution conformations and pH and ionic strength dependences of the conformations of two related mainly polyala peptides AP and AEP. The AP peptide sequence is $A_8RAA_3RA_4RA_2$ while the AEP sequence is $A_8ARA_3EA_4RA_2$. We tested the hypothesis that the Arg-10 and Glu-14 salt bridge would form in AEP and would stabilize the α-helix conformation. This hypothesis was based on previous studies that showed the impact of salt bridges on the α-helix conformation.[8−15,40−42] These studies indicated that oppositely charged side chains located at positions i and $i + 4$ should stabilize α-helices by ~ -2 kJ·mol^{-1},[43] while an i and $i + 3$ spacing should show a significantly smaller stabilization energy; while an i and $i + 5$ spacing should show negligible stabilization. For titratable side chains, the stabilization will also depend upon pH, as well as, the solution ionic strength.

Surprisingly, we find that the Glu substitution in AEP does not enhance α-helix stability. Instead, it results in a similar α-helix content as in AP, but shifts the α-helix length distribution toward more numerous, but smaller length α-helix segments; AEP, thus, has an increased concentration of α-helix-turn-α-helix conformations.

EXPERIMENTAL SECTION

Materials. The AP peptide ($A_8RA_4RA_4RA_2$, >95% purity) and the AEP peptide ($A_9RA_3EA_4RA_2$, >95% purity) were synthesized by Anaspec Inc. Sodium hydroxide (97%+) was purchased from Sigma, hydrochloric acid (36.5−38%) was purchased from J.T. Baker, and sodium chloride (AR) was purchased from Mallinckrodt. All chemicals were used as received. The sample pH was adjusted by adding HCl or NaOH solution. The volume added was less than 1% of the sample solution.

Received: December 23, 2010
Revised: February 28, 2011
Published: March 22, 2011

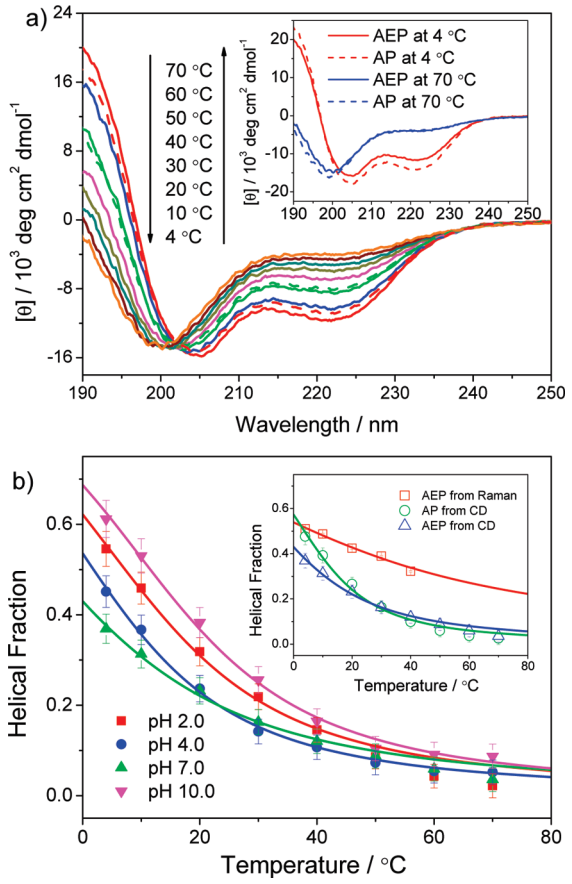

Figure 1. (a) Temperature dependence of CD spectra of AEP at pH 7.0. The solid lines indicate the heating process, the dashed lines indicate spectra measured after cooling. The inset compares CD spectra of AP and AEP. (b) Temperature dependent α-helical fraction and melting curves of AEP at different pH values. The α-helical fractions are calculated from the CD spectra by using eq 1. The melting curve is the fit of the temperature dependent α-helical fraction by using eq 3. The inset shows the AEP pH 7.0 melting curves calculated from CD and Raman spectra, and the AP pH 7.0 melting curve, calculated from the CD spectra.

Circular Dichroism Measurements. CD spectra were measured by using a Jasco J-710 spectrometer. We used temperature-controlled quartz cuvette of 0.2 mm (for 1.0 mg/mL samples) or 1 mm (for 0.2 mg/mL samples) path length. The CD spectra shown are the average of 10 scans.

UV Resonance Raman Spectra. The UVRR instrument was described in detail elsewhere.[44] The third harmonic of a Nd:YAG laser (Coherent Infinity) was anti-Stokes Raman shifted five harmonics in 40 psi hydrogen gas to 204 nm, which is in resonance with the peptide bond first allowed $\pi \rightarrow \pi^*$ transition. The backscattered Raman light was collected and dispersed with a partially subtractive double monochromator and detected by a Princeton Instruments Spec-10 CCD.

RESULTS AND DISCUSSION

Temperature Dependence of Conformational Transitions. Figure 1a shows the temperature dependence of the CD spectra of AEP at pH 7.0. The 4 °C spectrum shows two minima at ~222 and ~205 nm, which derive from the α-helix conformation.[45] These spectra clearly indicate a dominating α-helix conformation at 4 °C. As the temperature increases, the 222 nm trough becomes less evident, while the 205 nm minimum shifts to shorter wavelength due to α-helix melting. The temperature dependent spectra up to 50 °C show an isodichroic point at 202.4 nm, indicating that up to 50 °C the transition appears spectroscopically two-state. In contrast, the 60−70 °C spectra deviate from the isodichroic point, indicating formation of additional conformations. The high temperature AEP CD spectra look identical to those of AP, for which we have clearly demonstrated melting to a PPII-like conformation.[32]

The CD spectra of samples cooled from 70 to 20 °C and 4 °C show somewhat less negative ellipticities and troughs that are red-shifted by ~1 nm compared to the original 20 and 4 °C CD spectra. This suggests irreversible sample alterations due to the high temperature exposure.

The magnitude of the 222 nm CD band that is characteristic of α-helix conformations can be directly related to the fraction of α-helix-like conformations (f_H).

$$f_H = \frac{\theta - \theta_{PPII}}{\theta_\alpha - \theta_{PPII}} \quad (1)$$

where θ is the mean residue ellipticity at 222 nm, and θ_α and θ_{PPII} are the mean residue ellipticities at 222 nm of the α-helix and PPII-like conformations. Our previous AP study[29] showed that θ_α and θ_{PPII} are −26000 ± 1000 and −3200 ± 600 deg·cm^2·dmol^{-1}, respectively.

We calculated the Zimm−Bragg model nucleation parameter σ and propagation parameter s from the Figure 1 melting data. Here, σ is related to the likelihood of initiating an α-helical residue from a non-α-helix state and in the typical model is considered temperature independent. The term s is the ratio of the α-helix partition function to the non-α-helix partition function and is related to the enthalpy and entropy. If the partition function for the non-α-helix conformation is assigned a value of 1,

$$s = \exp\left(-\frac{\Delta h}{RT} + \frac{\Delta s}{R}\right) \quad (2)$$

where Δh and Δs are the enthalpy and entropy changes per residue, respectively, for the peptide bond to adopt an α-helix compared to a non-α-helix state. Statistical treatment with appropriate approximations gives the following quantitative melting curve:[46,47]

$$f_H = \frac{s}{(1+s) + \sqrt{(1-s)^2 + 4\sigma s}}\left(1 + \frac{(s-1) + 2\sigma}{\sqrt{(1-s)^2 + 4\sigma s}}\right) \quad (3)$$

Assuming that the α-helix is stabilized by interresidue hydrogen bonding, the thermodynamically least favored α-helix conformation would have a span of four α-helix residues. A four-residue α-helix span is too short to allow interresidue hydrogen bonding. Thus, this four α-helical residue conformation suffers an entropic penalty of $4\Delta s$ without any enthalpic hydrogen bonding compensation. On the basis of this argument, the temperature independent σ is calculated as

$$\sigma = \exp\left(\frac{4\Delta s}{R}\right) \quad (4)$$

The σ values obtained from the fitting our AEP data are comparable to those of previous studies[48,49] but somewhat larger

Table 1. Thermodynamic Parameters Obtained by Zimm−Bragg Model Fitting of the CD Melting Curves

peptide	ionic strength	pH	Δh/ kJ·mol^{-1}	Δs/ J·mol^{-1}·K^{-1}	T_m/°C	R^2
AP	0 M NaCl	7.0	−3.19 ± 0.05	−11.5 ± 0.2	4	0.985
AEP	0 M NaCl	2.0	−3.10 ± 0.03	−11.0 ± 0.1	9	0.994
		4.0	−3.12 ± 0.03	−11.3 ± 0.1	3	0.996
		7.0	−2.82 ± 0.04	−10.5 ± 0.1	−5	0.993
		10.0	−3.15 ± 0.03	−11.1 ± 0.1	11	0.994
	1.0 M NaCl	2.0	−3.18 ± 0.04	−11.0 ± 0.1	16	0.992
		4.0	−3.20 ± 0.03	−11.2 ± 0.1	13	0.995
		7.0	−3.08 ± 0.05	−10.9 ± 0.2	9	0.985
		10.0	−3.08 ± 0.08	−11.0 ± 0.3	7	0.969

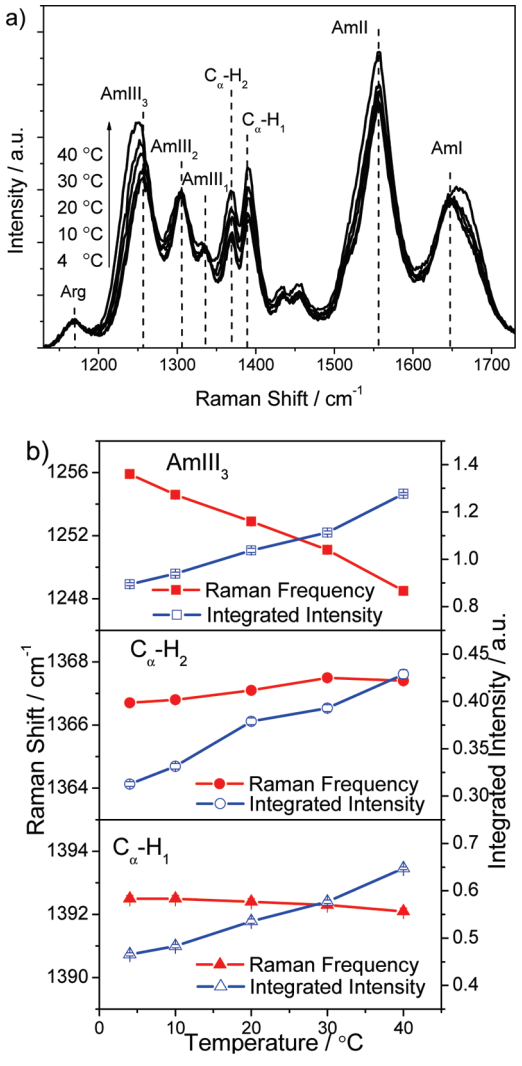

Figure 2. (a) Temperature dependence of UVRR spectra of AEP at pH 7.0. (b) AmIII$_3$ and C$_\alpha$−H band frequencies and integrated intensities from deconvolution of UVRR spectra. The error bars shown are standard deviations from the deconvolution.

than values obtained from the host−guest methods.[50,51] It should be noted that these host−guest method results have been questioned because poly(hydroxybutyl- or hydroxypropyl-)-L-glutamine hosts strongly favor formation of long α-helices

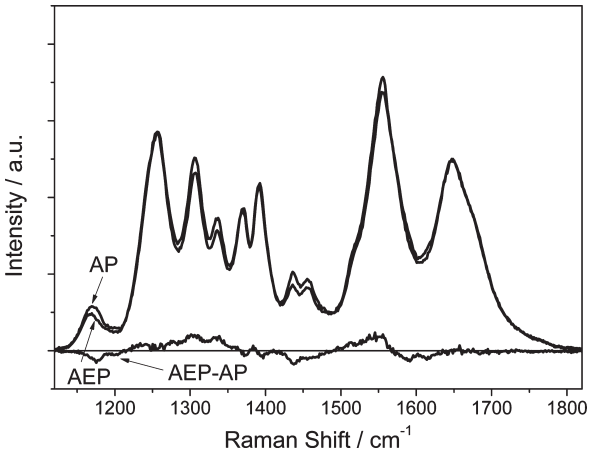

Figure 3. UV resonance Raman spectra of AEP and AP and their difference spectrum at 4 °C, pH 7.0.

and thus distort the estimation of σ values of the guest residues.[48,49,52]

When $s = 1$, T_m, the midpoint of the melting curve is

$$T_m = \frac{\Delta h}{\Delta s} \quad (5)$$

Figure 1b shows the best fits of the temperature dependence of the calculated α-helix fractions between 4 and 50 °C. The 60 and 70 °C data were not included because of the irreversible changes found upon high temperature incubation. The fitted thermodynamic parameters Δh, Δs, and T_m are listed in Table 1. These Δh and Δs values are close to those found in earlier studies[53−55] but are significantly smaller than those found recently.[31,37,48] Also, the T_m values obtained from these fits are systematically smaller.[31,37,48] This discrepancy might arise from the previous model which only permitted a single α-helix segment per peptide, which was thought to be reasonable for these short peptides. This approximation, as discussed below, appears inappropriate for our AEP peptide.

The hydrogen bonding enthalpy is expected to dominate Δh, but a relatively small hydrophobic contribution also occurs. A peptide chain of m α-helix segments of segment length L_m results in a total number of hydrogen bonds of $\Sigma L_m - 4m$, since each α-helix segment forms $L_m - 4$ hydrogen bonds. The zipper model assumes only one helix segment per peptide such that all helical peptide bonds are counted within one segment. This overcounts the number of hydrogen bonds as $\Sigma L_m - 4$. As a consequence, Δh is overestimated by $4(m - 1)$ hydrogen bond enthalpies.[56] The zipper model may also overestimate Δs, since the entropy of α-helical terminal residues is somewhat greater than those of the central residues. The overestimation of Δs, however, is likely to be smaller than the overestimation of Δh; this may bias the zipper model calculated T_m toward higher temperature.

Figure 2a shows the temperature dependence of the UVRR spectra of AEP between 4 and 40 °C at pH 7.0. These spectra are very similar to those of AP (Figure 3). At 4 °C, the broad band at ∼1650 cm^{-1} is composed of at least two overlapping bands: the AmI band at ∼1661 cm^{-1} and a 1645 cm^{-1} band which arises from the CN_3 asymmetric stretch of the guanidinium group of the Arg side chains. The AmII band occurs at ∼1556 cm^{-1}. The C$_\alpha$−H b bands occur at ∼1367 and ∼1392 cm^{-1}. The intensities

of the $C_\alpha-H$ b bands are inversely proportional to the α-helical fraction.[30,36,57] The $AmIII_1$ band occurs at ~1338 cm^{-1}, the $AmIII_2$ band occurs at ~1307 cm^{-1}, and the $AmIII_3$ band occurs at ~1256 cm^{-1}. The ~1170 cm^{-1} band consists of multiple contributions and involves NH_2 rocking of the Arg side chain guanidinium group, which makes this band sensitive to the environment, especially hydrogen bonding. Thus, this band is potentially useful for identifying the environment of Arg side chains.

The Figure 2a spectra show that, as the temperature increases, the two $C_\alpha-H$ bands become more intense, due to melting of the α-helix and formation of PPII-like conformations (Figure 2b). The $AmIII_3$ band downshifts, and its intensity increases. In contrast, the $AmIII_1$ band becomes weaker, whereas the $AmIII_2$ band shows little change. The similarity of the AEP and AP UVRR temperature dependence allows us to ascribe the observed AEP spectral changes to the melting of the α-helix to PPII-like conformations.

Comparison between AEP and AP. The CD spectra calculated α-helical fraction, f_H, of the 4 °C, pH 7.0 AEP sample (Figure 1) is smaller (0.37 ± 0.03) than that of AP (0.48 ± 0.04). In contrast, the Figure 3 UVRR spectra of AEP and AP in the AmIII and $C_\alpha-H$ b regions are essentially identical, indicating identical Ramachandran ψ angle distributions of AP and AEP. This indicates identical conformational distributions and identical helical fractions, in contrast to the CD results.

This disagreement results from the different mechanisms of CD and Raman spectroscopy. The CD phenomenon results from the coupling of electric and magnetic dipole transition moments whose values increase surpralinearly with the α-helix length.[58−60] Thus, the CD signal per peptide bond is stronger for long α-helices and weaker for shorter helices. We previously estimated that the mean residue ellipticity at 222 nm changed from $\sim -3000° \cdot cm^2 \cdot dmol^{-1} \cdot res^{-1}$ for a fully unfolded peptide to $\sim -4000° \cdot cm^2 \cdot dmol^{-1} \cdot res^{-1}$ when the peptide adopts only a single α-helix turn.[61]

In contrast to CD, UVRR of peptide bonds show a more linear intensity dependence since each peptide bond independently contributes to the $AmIII_3$ and the $C_\alpha-H$ b band intensities.[35,62,63] The only nonlinear dependence of the UVRR band peptide bond cross sections results from a bias against long α-helices due to the decrease in electronic transition oscillator strength because of the hypochromism which results from excitonic interactions between the transition dipoles of adjacent peptide bonds in the α-helix conformation.[64,65] Since the Raman scattering cross section is roughly proportional to the square of the absorptivity, the α-helix Raman cross sections per α-helix peptide bonds will decrease for longer helices that have more excitonic interactions.

Considering the CD and Raman results together, we conclude that AEP has essentially the same α-helix fraction as AP, but differs in that it adopts more α-helix segments of shorter length than does AP; molecular dynamics simulation of polyala peptides found that α-helix-turn-α-helix conformations are common.[56,66,67]

Recent MD simulation by Zhang et al. showed that the Fs peptide (which has the same sequence as AP, but is capped by acetyl and amide groups) forms both a single α-helix and α-helix-turn-α-helix conformation.[67] Due to the lower intrinsic α-helical propensity of the AEP Glu-14 than that of Arg-14 in AP,[68] it is likely that AEP forms more α-helix-turn-α-helix conformations, with the turn structures occurring around Glu-14. The α-helix segment between Glu-14 and the C-terminus is probably too short to contribute much of a CD signature, whereas this short segment contributes well to the UVRR.

AEP has two Arg compared to the three of AP. Thus, unless there is a conformational dependence of the Arg Raman intensities, the ~1170 cm^{-1} Arg band intensity should decrease by a third in AEP. However, Figure 3 shows that the AEP Arg band intensity decreases by only 20% and its frequency downshifts in AEP from that in AP demonstrating that the Arg Raman cross section and band frequencies depend upon the side chain environment and peptide conformation.

The ~1170 cm^{-1} Arg band appears to consist of, at least, two components (Figure 3), which presumably result from Arg side chains in different environments. One component probably arises from Arg side chains completely accessible to water. A fully hydrated Arg would occur, for example, in the extended PPII-like conformation. The other component probably results from a partially hydrated state where the Arg side chain occurs in a more folded state, such as in an α-helix-like conformation. In the α-helix-like conformation, the Arg side chain would be partially shielded from water by the backbone, preventing full hydrogen bonding between water and the guanidinium group. In addition, in the α-helix, the peptide bond carbonyls are intramolecularly hydrogen bonded to the peptide bond NH groups, which prevent hydrogen bonding between the guanidinium and peptide bond carbonyls.

pH and Ionic Strength Dependence of AEP Conformations. The helix stability is determined by the helix propensities of the amino acids and the possible interactions between the side chains and the macro-dipole.[68] The Gibbs free energy change for the conversion of the unfolded conformation to the α-helix conformation (U → H)

$$\Delta G_{U\rightarrow H} = \sum_{AA} \Delta G^{AA}_{U\rightarrow H} + \Delta G^{ND}_{U\rightarrow H} + \Delta G^{CD}_{U\rightarrow H} + \sum_{SD} \Delta G^{SD}_{U\rightarrow H} + \Delta G^{CR}_{U\rightarrow H} + \Delta G^{SB}_{U\rightarrow H} + \sum_{SS} \Delta G^{SS}_{U\rightarrow H} \quad (6)$$

$\Sigma_{AA}\, \Delta G^{AA}_{U\rightarrow H}$ is the summation of the α-helix propensity contributions to the α-helix stability of all the residues; $\Delta G^{ND}_{U\rightarrow H}$ is the contribution from the electrostatic interaction between the N-terminal amino group (α-NH_3^+) and the α-helix macro-dipole; $\Delta G^{CD}_{U\rightarrow H}$ is the contribution from the electrostatic interaction between the C-terminal carboxylate (α-COO^-) and the α-helix macro-dipole; $\Sigma_{SD}\Delta G^{SD}_{U\rightarrow H}$ is the summation of the contributions from the electrostatic interactions between charged side chains (Arg-10, Arg-19, and Glu-14, if charged) and the α-helix macro-dipole; $\Delta G^{CR}_{U\rightarrow H}$ is the contribution from the electrostatic interaction between the Arg-19 side chain guanidinium cation and the α-helix C-terminal anion; $\Delta G^{SB}_{U\rightarrow H}$ is the contribution from the possible salt bridge formation between the Arg-10 and Glu-14 side chains, including the contribution of a hydrogen bond from the Arg guanidinium to the Glu carboxylate; $\Sigma_{SS}\Delta G^{SS}_{U\rightarrow H}$ is the summation of contributions to the α-helix stability from side chain−side chain interactions except for the possible salt bridge.

These electrostatic interactions depend upon the solution pH and ionic strength; the charge states of AEP depend upon pH. These different charge states show different α-helix stabilizations/destabilizations. In order to study the impact of pH on α-helix stability, we measured the pH dependence of the α-helical fraction of AEP at 4 °C by using CD and UVRR spectroscopy.

In AEP, there are three titratable groups: the C-terminal carboxyl, the Glu-14 side chain carboxyl, and the N-terminal amine. Therefore, there are four charge states in AEP. The

Scheme 1. Species in AEP Solution[a]

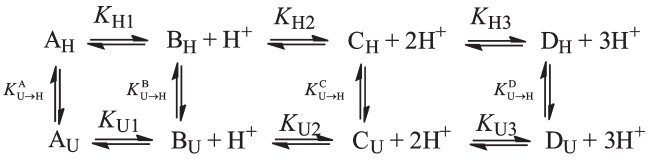

A: $^{+}$AAAAAAAAAR^{+}AAAE^{0}AAAAR^{+}AA^{0}
B: $^{+}$AAAAAAAAAR^{+}AAAE^{0}AAAAR^{+}AA^{-}
C: $^{+}$AAAAAAAAAR^{+}AAAE^{-}AAAAR^{+}AA^{-}
D: ^{0}AAAAAAAAAR^{+}AAAE^{-}AAAAR^{+}AA^{-}

[a] The subscripts H and U represent α-helix and unfolded conformations.

Table 2. Equilibrium Constants Obtained by Fitting the CD and Raman pH Dependent Helical Fractions with Equation 7

α-helical formation equilibrium constant[a]	CD	Raman
$K^A_{U\to H}$	1.2 ± 0.2	1.44 ± 0.02
$K^B_{U\to H}$	0.68 ± 0.10	1.04 ± 0.02
$K^C_{U\to H}$	0.58 ± 0.08	1.04 ± 0.01
$K^D_{U\to H}$	1.8 ± 0.3	1.89 ± 0.02
pK_a[b]	**CD**	**Raman**
pK_{H1}	3.4 ± 0.2	4.0 ± 0.2
pK_{H2}	7.0 ± 2.0	7.7 ± 1.9
pK_{H3}	7.4 ± 0.2	7.4 ± 0.3
ΔpK_a ($pK_H - pK_U$)[c]	**CD**	**Raman**
ΔpK_{a1}	0.2 ± 0.1	0.14 ± 0.01
ΔpK_{a2}	0.1 ± 0.1	0.00 ± 0.01
ΔpK_{a3}	−0.5 ± 0.1	−0.30 ± 0.01

[a] Measured equilibrium constants, which are fixed in fitting. The errors are experimental standard deviations. [b] Errors are standard deviations from fitting. [c] Errors calculated from the errors of α-helical formation equilibrium constants.

peptide in each charge state will occur in different α-helix/unfolded conformation equilibria due to the different α-helix stabilization/destabilization. Scheme 1 defines these states and the transitions between them.

The pH dependent α-helical fraction of AEP is given by (See the Appendix for derivation):

$$f_H = [1 + 10^{pH - pK_{H1}} + 10^{2pH - pK_{H1} - pK_{H2}} + 10^{3pH - pK_{H1} - pK_{H2} - pK_{H3}}]/[(1 + 1/K^A_{U\to H}) + (1 + 1/K^B_{U\to H})10^{pH - pK_{H1}} + (1 + 1/K^C_{U\to H})10^{2pH - pK_{H1} - pK_{H2}} + (1 + 1/K^D_{U\to H})10^{3pH - pK_{H1} - pK_{H2} - pK_{H3}}] \quad (7)$$

The pK_{H1}, pK_{H2}, and pK_{H3} terms are the pK_a of the C-terminal carboxyl, the Glu-14 side chain carboxyl, and the N-terminal amine in the α-helix conformations. The α-helical formation equilibrium constants $K^A_{U\to H}$, $K^B_{U\to H}$, $K^C_{U\to H}$, and $K^D_{U\to H}$ were obtained from the CD and the UVRR data.

At pH 2.0, the C-terminal and Glu-14 side chain carboxyls are protonated and neutral, while the N-terminal amino group is protonated and cationic. This corresponds to state A in Scheme 1. The concentrations of other charged states are negligible. Therefore, $K^A_{U\to H} = f_H(2.0)/(1-f_H(2.0))$.

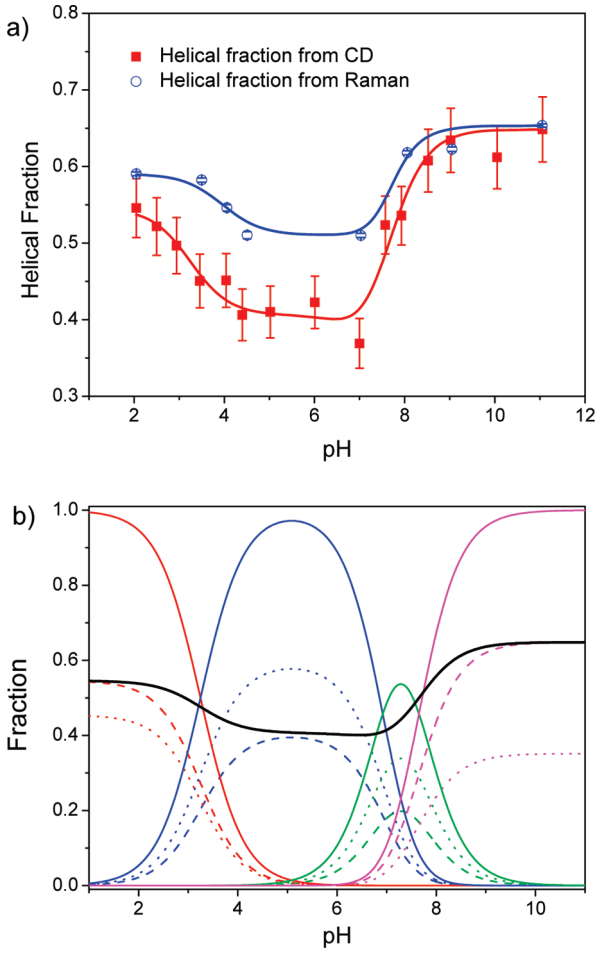

Figure 4. (a) pH dependence of helical fraction, f_H, of AEP at 4 °C in pure water calculated from the CD and UVRR spectra via eq 1. The curves show the fit to eq 7. (b) Calculated AEP species fractions from CD spectra (see Scheme 1): (red) state A, (blue) state B, (green) state C, (magenta) state D; (dashed lines) α-helix conformation, (dotted lines) unfolded conformation, (solid lines) total AEP fraction in each state including helix and unfolded conformations; (thick solid black line) total helical fraction.

At pH 4.5, the C-terminal carboxyl is mainly deprotonated, while the Glu-14 side chain carboxyl and N-terminal amino group remain protonated. This corresponds to state B. Therefore, $K^B_{U\to H} = f_H(4.5)/(1-f_H(4.5))$.

At pH 7.0, state C with two carboxylates and a protonated N-terminal amino group is the major AEP component. Thus $K^C_{U\to H} = f_H(7.0)/(1-f_H(7.0))$.

At pH 11.0, state D dominates, where all titratable groups are deprotonated. Therefore, $K^D_{U\to H} = f_H(11.0)/(1-f_H(11.0))$.

The values of these α-helical formation equilibrium constants calculated from the CD and UVRR data are listed in Table 2. We fitted the experimental α-helical fraction data calculated from the CD and UVRR spectra, to eq 6 using the corresponding measured $K^A_{U\to H}$, $K^B_{U\to H}$, $K^C_{U\to H}$, and $K^D_{U\to H}$ values (Figure 4a). The fitting results are listed in Table 2.

In the conversion from state B to state C, the Glu-14 is deprotonated and a salt bridge may form. In state C, there may be an interaction between the Glu-14 charge and the macro-dipole. The helix propensity for the state C deprotonated Glu-14 differs from that of the state B protonated Glu-14. Except for the possible

dx.doi.org/10.1021/jp112238q |J. Phys. Chem. B 2011, 115, 4234–4243

salt bridge formation, the interaction between the Glu-14 and the marco-dipole and the helix propensity difference, all other interactions not involving Glu-14 should be identical for states B and C. The states B and C Gibbs free energy changes for the conversion from the unfolded conformation to the α-helix conformation can be written as follows:

$$\begin{aligned}\Delta G^{B}_{U\rightarrow H} &= \sum_{AA'}\Delta G^{AA'}_{U\rightarrow H} + \Delta G^{E^0}_{U\rightarrow H} + \Delta G^{ND}_{U\rightarrow H} + \Delta G^{CD}_{U\rightarrow H} \\ &+ \sum_{SD'}\Delta G^{SD'}_{U\rightarrow H} + \Delta G^{CR}_{U\rightarrow H} + \sum_{SS}\Delta G^{SS}_{U\rightarrow H}\Delta G^{C}_{U\rightarrow H} \\ &= \sum_{AA'}\Delta G^{AA'}_{U\rightarrow H} + \Delta G^{E^-}_{U\rightarrow H} + \Delta G^{ND}_{U\rightarrow H} + \Delta G^{CD}_{U\rightarrow H} \\ &+ \sum_{SD'}\Delta G^{SD'}_{U\rightarrow H} + \Delta G^{E^-D}_{U\rightarrow H} + \Delta G^{CR}_{U\rightarrow H} \\ &+ \Delta G^{SB}_{U\rightarrow H} + \sum_{SS}\Delta G^{SS}_{U\rightarrow H} \end{aligned} \quad (8)$$

The helix propensities of the state B protonated Glu-14 and the state C deprotonated Glu-14 are explicitly separated from those of the other residues, which are denoted as AA′. The summation over SD′ denotes the interactions between the Arg-10 and Arg-19 charges and the macro-dipole; $\Delta G^{E^-D}_{U\rightarrow H}$ is the contribution from the interaction between the Glu-14 charge and the macro-dipole. By taking the difference between states B and C

$$\begin{aligned}\Delta G^{C}_{U\rightarrow H} - \Delta G^{B}_{U\rightarrow H} &= \Delta G^{SB}_{U\rightarrow H} + \Delta G^{E^-D}_{U\rightarrow H} \\ &+ (\Delta G^{E^-}_{U\rightarrow H} - \Delta G^{E^0}_{U\rightarrow H}) \end{aligned} \quad (9)$$

By rearranging, we obtain the following:

$$\begin{aligned}\Delta G^{SB}_{U\rightarrow H} + \Delta G^{E^-D}_{U\rightarrow H} &= (\Delta G^{C}_{U\rightarrow H} - \Delta G^{B}_{U\rightarrow H}) \\ &- (\Delta G^{E^-}_{U\rightarrow H} - \Delta G^{E^0}_{U\rightarrow H}) \end{aligned} \quad (10)$$

The two Gibbs free energy differences in the second term are expected to be 1.81 kJ·mol^{-1} for $\Delta G^{E^-}_{U\rightarrow H}$ and 0.941 kJ·mol^{-1} for $\Delta G^{E^0}_{U\rightarrow H}$ (values for $\Delta G^{E^-}_{U\rightarrow H}$ and $\Delta G^{E^0}_{U\rightarrow H}$ are taken from Table 2 of ref 68). $\Delta G^{B}_{U\rightarrow H}$ and $\Delta G^{C}_{U\rightarrow H}$ can be calculated from the measured α-helical formation equilibrium constant $K^{B}_{U\rightarrow H}$ and $K^{C}_{U\rightarrow H}$ for states B and C

$$\begin{aligned}\Delta G^{B}_{U\rightarrow H} &= -RT\ln K^{B}_{U\rightarrow H} \\ \Delta G^{C}_{U\rightarrow H} &= -RT\ln K^{C}_{U\rightarrow H} \end{aligned} \quad (11)$$

We, thus, obtain a value $\Delta G^{SB}_{U\rightarrow H} + \Delta G^{E^-D}_{U\rightarrow H} = -0.5 \pm 0.5$ kJ·mol^{-1}, which indicates that the salt bridge, together with the interaction between Glu-14 charge and macro-dipole, probably has little impact on the α-helix stability.

We can estimate the contribution from the interaction between the C-terminal carboxylate charge and the macro-dipole ($\Delta G^{CD}_{U\rightarrow H}$), plus the interaction between the C-terminal carboxylate charge and the Arg-19 side chain ($\Delta G^{CR}_{U\rightarrow H}$) to the α-helix stability, as well as the contribution from the interaction between the N-terminal amino charge and the macro-dipole ($\Delta G^{ND}_{U\rightarrow H}$) to the α-helix stability.

$$\begin{aligned}\Delta G^{CD}_{U\rightarrow H} + \Delta G^{CR}_{U\rightarrow H} &= \Delta G^{B}_{U\rightarrow H} - \Delta G^{A}_{U\rightarrow H} = -RT(\ln K^{B}_{U\rightarrow H} \\ &- \ln K^{A}_{U\rightarrow H})\Delta G^{ND}_{U\rightarrow H} = \Delta G^{C}_{U\rightarrow H} - \Delta G^{D}_{U\rightarrow H} = \\ &- RT(\ln K^{C}_{U\rightarrow H} - \ln K^{D}_{U\rightarrow H}) \end{aligned} \quad (12)$$

From the above equations, we estimate that $\Delta G^{CD}_{U\rightarrow H} + \Delta G^{CR}_{U\rightarrow H} = 1.3 \pm 0.5$ kJ·mol^{-1}; $\Delta G^{ND}_{U\rightarrow H} = 2.6 \pm 0.5$ kJ·mol^{-1}. These two values are significantly larger than $\Delta G^{SB}_{U\rightarrow H} + \Delta G^{E^-}_{U\rightarrow H}{}^{D}$, indicating that these unfavorable interactions have greater impact on the α-helix stability than does the favorable salt bridge.

These results explain the pH dependences of helical fraction: at low or high pH, AEP has a higher α-helical fraction than at neutral pH. The deprotonation of C-terminal carboxyl, which turns on the interaction between the C-terminal carboxylate charge and the macro-dipole ($\Delta G^{CD}_{U\rightarrow H}$), as well as, the interaction between the C-terminal carboxylate charge and the Arg-19 side chain ($\Delta G^{CR}_{U\rightarrow H}$), destabilize the α-helix. At high pH, the neutralization of the N-terminal amino, which eliminates the interaction between the N-terminal amino charge and the macro-dipole ($\Delta G^{ND}_{U\rightarrow H}$) stabilizes the α-helix. Because the C-terminal carboxyl and N-terminal amino are involved in the interactions that affect the α-helix stability, their pK_a values differ between the unfolded and the α-helix conformations. The pK_a differences between the α-helix conformation and the unfolded conformation (ΔpK_a = pK_H − pK_U) calculated from the α-helical formation equilibrium constants are listed in Table 2 (see the Appendix for details).

We also can calculate $\Delta G^{SB}_{U\rightarrow H} + \Delta G^{E^-D}_{U\rightarrow H}$, $\Delta G^{CD}_{U\rightarrow H} + \Delta G^{CR}_{U\rightarrow H}$, and $\Delta G^{ND}_{U\rightarrow H}$ from the UVRR spectra. The C_α−H b bands derive from the PPII-like conformations. Thus, the integrated intensity of the C_α−H b band is proportional to the PPII fraction. By assuming a two-state transition, we can calculate the helical fraction from the UVRR spectra. At pH 7.0 and 4 °C, AEP has the identical C_α−H b band intensity as does AP (Figure 3), indicating identical helical fractions of ∼0.51;[29,37] at pH 7.0 and 4 °C, AEP has a PPII fraction of ∼0.49. We therefore calculate the PPII fractions of AEP at other pH values by the proportionality between the PPII fraction and the C_α−H b bands integrated intensity and subsequently calculate the pH dependent helical fractions.

Figure 4a shows the calculated pH dependence of the AEP helical fraction calculated from the CD and Raman spectra. By applying the procedure to the Raman results, we calculated that $\Delta G^{SB}_{U\rightarrow H} + \Delta G^{E^-D}_{U\rightarrow H} = -0.9 \pm 0.1$ kJ·mol^{-1}, $\Delta G^{CD}_{U\rightarrow H} + \Delta G^{CR}_{U\rightarrow H} = 0.8 \pm 0.1$ kJ·mol^{-1}, and $\Delta G^{ND}_{U\rightarrow H} = 1.4 \pm 0.1$ kJ·mol^{-1}. These values are somewhat different than the values obtained from the CD spectra, due to the fact that the CD is biased toward smaller α-helix fraction as discussed above.

Table 1 shows our CD calculated average residue enthalpy changes (Δh) and entropy changes (Δs) (also shown in Figure 5b) as well as T_m. These thermodynamic parameters, Δh and Δs, are for the transition from the unfolded to the α-helix conformation at specific pH values and ionic strengths. Figure 5b shows that Δh and Δs at pH 7.0 are more positive than at other pH values due to the two α-helix destabilizing terminal charge−macro-dipole (C-terminal−macro-dipole and N-terminal−macro-dipole) interactions. At pH 2.0 and 10.0, only a single unfavorable terminal charge−macro-dipole interaction occurs.

The smaller T_m and Δh of AEP compared to those of AP at pH 7.0 can be explained by more α-helix-turn-α-helix conformations in AEP. The peptide bonds at both ends of an α-helix segment can only form single intrapeptide hydrogen bonds. Thus, the average Δh should be more positive for α-helix-turn-α-helix conformations than for the same total number of α-helical residues within a single helix segment.

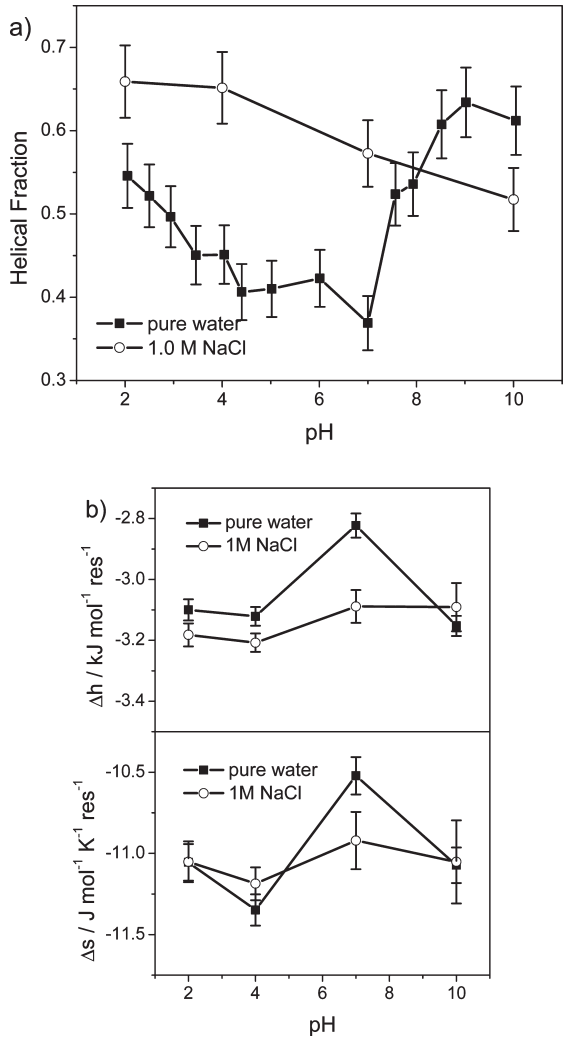

Figure 5. (a) pH dependence of the α-helical fraction, f_H, of AEP at 4 °C in pure water and 1.0 M NaCl. (b) pH dependence of average enthalpy change (Δh) and entropy change (Δs) per residue for forming an α-helical peptide bond conformation at 4 °C in pure water and in 1.0 M NaCl. See Table 1.

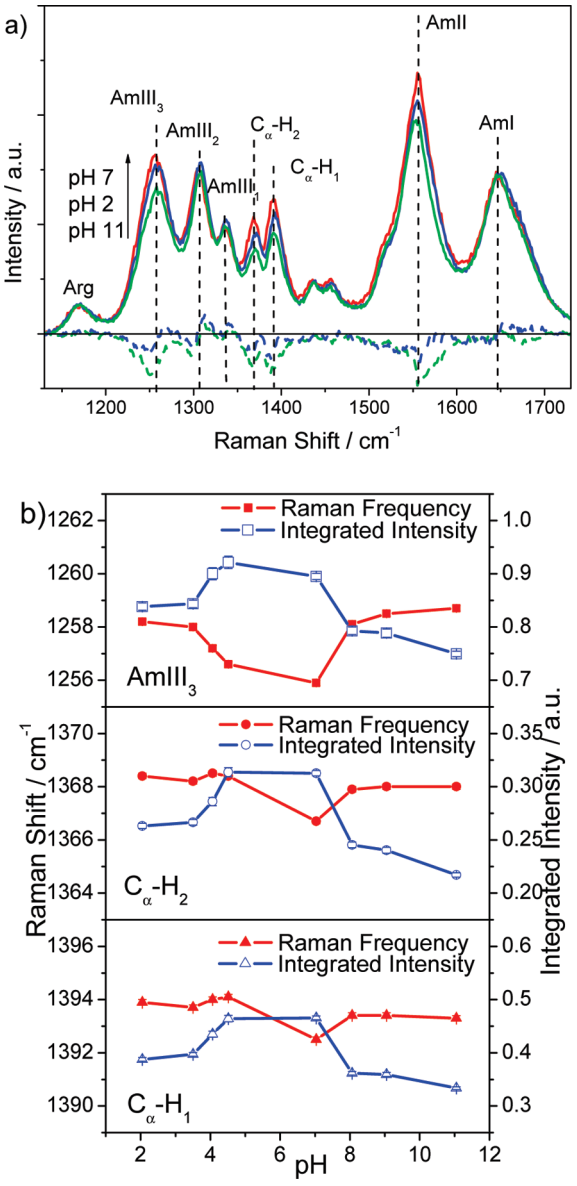

Figure 6. (a) pH dependence of AEP UVRR spectra at 4 °C. (b) pH dependence of $AmIII_3$ and C_α−H band frequencies and integrated intensities from deconvolution of UVRR spectra. The error bars shown are standard deviations from the deconvolution.

The interactions between charges as well as between charges and the α-helix macro-dipole are electrostatic and therefore can be screened by high ionic strength. We increased the sample ionic strength by adding 1.0 M NaCl. As expected, the high ionic strength solution showed a smaller dependence of f_H, T_m, Δh, and Δs on pH (Table 1 and Figure 5).

Figure 6a shows the pH dependence of the AEP UVRR spectra at 4 °C. The intensities of the $AmIII_3$ and C_α−H b bands are larger at pH 7.0 than at pH 2.0 or 11.0, while the $AmIII_3$ frequency varies by <4 cm^{-1} (Figure 6b). The increased C_α−H b and $AmIII_3$ band intensities at pH 7.0 clearly signal the melting of the α-helix conformation. However, the lack of an $AmIII_3$ band frequency shift indicates that the melting is not to a PPII-like conformation, but the melting occurs to conformations with similar Ramachandran Ψ angles to that of the α-helix.

AEP forms α-Helix-Turn-α-Helix Conformation. Both the pH 2.0−7.0 and pH 11.0−7.0 UVRR difference spectra show a negative trough at ~1251 cm^{-1}, from which we can calculate the Ramachandran Ψ angle.[36] Since the hydrogen bonding status of the residues is unknown, we estimate the Ψ angle by using eq 6E in ref 36 and obtain a value of −27°. A perfect type III turn has an Ψ angle of −30°. Therefore, the negative trough of 1251 cm^{-1} suggests that at pH 7.0, the AEP α-helix partially melts to a type III turn-like structure. This type III turn-like structure is likely to occur around the Glu-14, because the helix propensity of Glu is lower than those of Ala and Arg.[68,69]

Figure 4a compares the pH dependences of AEP helical fractions obtained from CD and UVRR. At low or high pH, the helical fractions calculated from CD and UVRR spectra are similar. At neutral pH, there is a significant discrepancy between helical fractions calculated from the CD and UVRR spectra. As discussed previously, the similar α-helix content measured by CD and UVRR at low and high pH indicates that at these pH values AEP adopts long helical segments that have large CD

ellipticities. The large discrepancy at neutral pH indicates that the α-helix forms multiple short helices that only show small ellipticities and thus bias the CD measurement toward small α-helical contents. Therefore, we conclude that at low and high pH, AEP has less turn structures and a longer α-helix segment. At neutral pH, AEP has more turn structures and shorter α-helix segments.

CONCLUSIONS

We compared the polyala peptide AP that has three Arg side chains to the peptide AEP where Arg-14 is replaced with a Glu. We find that the AEP peptide has an increased concentration of α-helix-turn-α-helix conformations. We examined the nature of the electrostatic interactions that (de)stabilize α-helix conformations. The inter-residue interactions between the Arg-10 and Glu-14 in AEP make only a minor contribution to the α-helix stabilization. As the temperature increases, the AEP melts from α-helix to PPII-like conformations, while the pH induced melting causes the formation of an α-helix-type III turn-α-helix conformation.

APPENDIX

Derivation of Equation 7. In Scheme 1, the α-helical fraction of AEP is a function of pH:

$$f_H = [A_H] + [B_H] + [C_H] + [D_H] \quad (A1)$$

where $[A_H]$, $[B_H]$, $[C_H]$, and $[D_H]$ are the helical fractions in states A, B, C, and D. For each charge state, the relationship between the α-helix conformation and the unfolded conformation is given by

$$\begin{aligned} [A_U] &= \frac{[A_H]}{K^A_{U\to H}} \\ [B_U] &= \frac{[B_H]}{K^B_{U\to H}} \\ [C_U] &= \frac{[C_H]}{K^C_{U\to H}} \\ [D_U] &= \frac{[D_H]}{K^D_{U\to H}} \end{aligned} \quad (A2)$$

The peptide concentration is conserved in solution, therefore,

$$[A_H] + [A_U] + [B_H] + [B_U] + [C_H] + [C_U] + [D_H] + [D_U] = 1 \quad (A3)$$

Substituting eq A2 into eq A3, we eliminate four unknowns:

$$\begin{aligned} &(1 + 1/K^A_{U\to H})[A_H] + (1 + 1/K^B_{U\to H})[B_H] \\ &+ (1 + 1/K^C_{U\to H})[C_H] + (1 + 1/K^D_{U\to H})[D_H] \\ &= 1 \end{aligned} \quad (A4)$$

The Henderson−Hasselbalch equation gives relationships between two adjacent states:

$$\begin{aligned} [B_H] &= [A_H] \times 10^{pH - pK_{H1}} \\ [C_H] &= [B_H] \times 10^{pH - pK_{H2}} \\ [D_H] &= [C_H] \times 10^{pH - pK_{H3}} \end{aligned} \quad (A5)$$

Combining eq A5 and eq A4, we obtain expressions for $[A_H]$, $[B_H]$, $[C_H]$, and $[D_H]$:

$$\begin{aligned} [A_H] &= 1/[(1 + 1/K^A_{U\to H}) + (1 + 1/K^B_{U\to H}) \times 10^{pH - pK_{H1}} \\ &\quad + (1 + 1/K^C_{U\to H})10^{2pH - pK_{H1} - pK_{H2}} \\ &\quad + (1 + 1/K^D_{U\to H})10^{3pH - pK_{H1} - pK_{H2} - pK_{H3}}] \\ [B_H] &= 10^{pH - pK_{H1}}/[(1 + 1/K^A_{U\to H}) + (1 + 1/K^B_{U\to H})10^{pH - pK_{H1}} \\ &\quad + (1 + 1/K^C_{U\to H})10^{2pH - pK_{H1} - pK_{H2}} \\ &\quad + (1 + 1/K^D_{U\to H})10^{3pH - pK_{H1} - pK_{H2} - pK_{H3}}] \\ [C_H] &= 10^{2pH - pK_{H1} - pK_{H2}}/[(1 + 1/K^A_{U\to H}) \\ &\quad + (1 + 1/K^B_{U\to H})10^{pH - pK_{H1}} \\ &\quad + (1 + 1/K^C_{U\to H})10^{2pH - pK_{H1} - pK_{H2}} \\ &\quad + (1 + 1/K^D_{U\to H})10^{3pH - pK_{H1} - pK_{H2} - pK_{H3}}] \\ [D_H] &= 10^{3pH - pK_{H1} - pK_{H2} - pK_{H3}}/[(1 + 1/K^A_{U\to H}) \\ &\quad + (1 + 1/K^B_{U\to H})10^{pH - pK_{H1}} \\ &\quad + (1 + 1/K^C_{U\to H})10^{2pH - pK_{H1} - pK_{H2}} \\ &\quad + (1 + 1/K^D_{U\to H})10^{3pH - pK_{H1} - pK_{H2} - pK_{H3}}] \end{aligned} \quad (A6)$$

Therefore, explicitly,

$$\begin{aligned} f_H &= [1 + 10^{pH - pK_{H1}} + 10^{2pH - pK_{H1} - pK_{H2}} \\ &\quad + 10^{3pH - pK_{H1} - pK_{H2} - pK_{H3}}]/[(1 + 1/K^A_{U\to H}) \\ &\quad + (1 + 1/K^B_{U\to H})10^{pH - pK_{H1}} \\ &\quad + (1 + 1/K^C_{U\to H})10^{2pH - pK_{H1} - pK_{H2}} \\ &\quad + (1 + 1/K^D_{U\to H})10^{3pH - pK_{H1} - pK_{H2} - pK_{H3}}] \end{aligned} \quad (A7)$$

Calculation of pK_a Difference (ΔpK_a) in Table 2. The calculations of ΔpK_{a1}, ΔpK_{a2}, and ΔpK_{a3} are similar. Here we only give the calculation of ΔpK_{a1} as an example. Consider the closed thermodynamic cycle of states A and B. The fraction of the unfolded conformation in state B can be calculated as follows:

$$[B_U] = \frac{[B_H]}{K^B_{U\to H}} = \frac{[A_H]10^{-pK_{H1}}}{[H^+]K^B_{U\to H}} \quad (A8)$$

However,

$$[B_U] = \frac{[A_U]}{[H^+]}10^{-pK_{U1}} = \frac{[A_H]10^{-pK_{U1}}}{[H^+]K^A_{U\to H}} \quad (A9)$$

Therefore,

$$\frac{[A_H]10^{-pK_{H1}}}{[H^+]K^B_{U\to H}} = \frac{[A_H]10^{-pK_{U1}}}{[H^+]K^A_{U\to H}} \quad (A10)$$

Eliminating $[A_H]$ and $[H^+]$ and rearranging eq A10

$$\frac{10^{-pK_{H1}}}{10^{-pK_{U1}}} = \frac{K^B_{U\to H}}{K^A_{U\to H}} \quad (A11)$$

$$10^{-(pK_{H1} - pK_{U1})} = \frac{K^B_{U\to H}}{K^A_{U\to H}} \quad (A12)$$

Substitute the definition of pK_a difference $\Delta pK_{a1} = pK_{H1} - pK_{U1}$ into eq A12:

$$\Delta pK_{a1} = \log_{10} K^A_{U\to H} - \log_{10} K^B_{U\to H} \quad (A13)$$

For $f(x) = \log_{10} x$, the uncertainty is $df(x) = dx/2.303x$; therefore,

the uncertainty of ΔpK_{a1} is

$$d(\Delta pK_{a1}) = \sqrt{\left(\frac{d(K_{U\rightarrow H}^{A})}{2.303K_{U\rightarrow H}^{A}}\right)^2 + \left(\frac{d(K_{U\rightarrow H}^{B})}{2.303K_{U\rightarrow H}^{B}}\right)^2} \quad \text{(A14)}$$

The calculations of ΔpK_{a2} and ΔpK_{a3} can be achieved by examining the closed thermodynamic cycles of states B and C and of states C and D.

■ ASSOCIATED CONTENT

Supporting Information. Temperature dependent CD spectra at pH 2, 4, and 10, as well as the pH dependent CD spectra at 4 °C. This information is available free of charge via the Internet at http://pubs.acs.org.

■ AUTHOR INFORMATION

Present Addresses

[†]Optical Technology Division, National Institute of Standards and Technology, Gaithersburgh, MD 20899.

■ ACKNOWLEDGMENT

We thank Dr. Bhavya Sharma, Lu Ma, and Dr. Edward Gooding for their helpful discussions. This work is supported by NIH Grant 5RO1 EB002053 and NIH 1RO1 EB009089.

■ REFERENCES

(1) Dill, K. A. *Protein Sci.* **1999**, *8* (6), 1166–1180.
(2) Dill, K. A.; Bromberg, S.; Yue, K. Z.; Fiebig, K. M.; Yee, D. P.; Thomas, P. D.; Chan, H. S. *Protein Sci.* **1995**, *4* (4), 561–602.
(3) Barlow, D. J.; Thornton, J. M. *J. Mol. Biol.* **1983**, *168*, 867–885.
(4) Horovitz, A.; Serrano, L.; Avron, B.; Bycroft, M.; Fersht, A. R. *J. Mol. Biol.* **1990**, *216*, 1031–1044.
(5) Hendsch, Z. S.; Tidor, B. *Protein Sci.* **1994**, *3* (2), 211–226.
(6) Musafia, B.; Buchner, V.; Arad, D. *J. Mol. Biol.* **1995**, *254* (4), 761–770.
(7) Kumar, S.; Nussinov, R. *J. Mol. Biol.* **1999**, *293* (5), 1241–1255.
(8) Marqusee, S.; Baldwin, R. L. *Proc. Natl. Acad. Sci. U. S. A.* **1987**, *84* (24), 8898–8902.
(9) Stellwagen, E.; Park, S. H.; Shalongo, W.; Jain, A. *Biopolymers* **1992**, *32* (9), 1193–1200.
(10) HuyghuesDespointes, B. M. P.; Scholtz, J. M.; Baldwin, R. L. *Protein Sci.* **1993**, *2* (1), 80–85.
(11) Scholtz, J. M.; Qian, H.; Robbins, V. H.; Baldwin, R. L. *Biochemistry* **1993**, *32* (37), 9668–9676.
(12) HuyghuesDespointes, B. M. P.; Baldwin, R. L. *Biochemistry* **1997**, *36* (8), 1965–1970.
(13) Smith, J. S.; Scholtz, J. M. *Biochemistry* **1998**, *37* (1), 33–40.
(14) Olson, C. A.; Spek, E. J.; Shi, Z. S.; Vologodskii, A.; Kallenbach, N. R. *Proteins* **2001**, *44* (2), 123–132.
(15) Errington, N.; Doig, A. J. *Biochemistry* **2005**, *44* (20), 7553–7558.
(16) Iqbalsyah, T. M.; Doig, A. J. *J. Am. Chem. Soc.* **2005**, *127* (14), 5002–5003.
(17) Park, S. H.; Shalongo, W.; Stellwagen, E. *Biochemistry* **1993**, *32* (47), 12901–12905.
(18) Mayne, L.; Englander, S. W.; Qiu, R.; Yang, J. X.; Gong, Y. X.; Spek, E. J.; Kallenbach, N. R. *J. Am. Chem. Soc.* **1998**, *120* (41), 10643–10645.
(19) Sindelar, C. V.; Hendsch, Z. S.; Tidor, B. *Protein Sci.* **1998**, *7* (9), 1898–1914.
(20) Fezoui, Y.; Braswell, E. H.; Xian, W. J.; Osterhout, J. J. *Biochemistry* **1999**, *38* (9), 2796–2804.
(21) Shi, Z. S.; Olson, C. A.; Bell, A. J.; Kallenbach, N. R. *Biopolymers* **2001**, *60* (5), 366–380.
(22) Garcia, A. E.; Sanbonmatsu, K. Y. *Proc. Natl. Acad. Sci. U. S. A.* **2002**, *99* (5), 2782–2787.
(23) Ghosh, T.; Garde, S.; Garcia, A. E. *Biophys. J.* **2003**, *85* (5), 3187–3193.
(24) Iqbalsyah, T. M.; Doig, A. J. *Biochemistry* **2005**, *44* (31), 10449–10456.
(25) Asher, S. A. *Anal. Chem.* **1993**, *65* (4), A201–A210.
(26) Asher, S. A. *Anal. Chem.* **1993**, *65* (2), A59–A66.
(27) Chi, Z. H.; Asher, S. A. *Biochemistry* **1998**, *37* (9), 2865–2872.
(28) Chi, Z. H.; Chen, X. G.; Holtz, J. S. W.; Asher, S. A. *Biochemistry* **1998**, *37* (9), 2854–2864.
(29) Lednev, I. K.; Karnoup, A. S.; Sparrow, M. C.; Asher, S. A. *J. Am. Chem. Soc.* **1999**, *121* (35), 8074–8086.
(30) Asher, S. A.; Ianoul, A.; Mix, G.; Boyden, M. N.; Karnoup, A.; Diem, M.; Schweitzer-Stenner, R. *J. Am. Chem. Soc.* **2001**, *123* (47), 11775–11781.
(31) Lednev, I. K.; Karnoup, A. S.; Sparrow, M. C.; Asher, S. A. *J. Am. Chem. Soc.* **2001**, *123* (10), 2388–2392.
(32) Asher, S. A.; Mikhonin, A. V.; Bykov, S. *J. Am. Chem. Soc.* **2004**, *126* (27), 8433–8440.
(33) Mikhonin, A. V.; Ahmed, Z.; Ianoul, A.; Asher, S. A. *J. Phys. Chem. B* **2004**, *108* (49), 19020–19028.
(34) Ahmed, Z.; Beta, I. A.; Mikhonin, A. V.; Asher, S. A. *J. Am. Chem. Soc.* **2005**, *127* (31), 10943–10950.
(35) Mikhonin, A. V.; Asher, S. A. *J. Phys. Chem. B* **2005**, *109* (7), 3047–3052.
(36) Mikhonin, A. V.; Bykov, S. V.; Myshakina, N. S.; Asher, S. A. *J. Phys. Chem. B* **2006**, *110* (4), 1928–1943.
(37) Mikhonin, A. V.; Asher, S. A. *J. Am. Chem. Soc.* **2006**, *128* (42), 13789–13795.
(38) Mikhonin, A. V.; Myshakina, N. S.; Bykov, S. V.; Asher, S. A. *J. Am. Chem. Soc.* **2005**, *127* (21), 7712–7720.
(39) Ma, L.; Ahmed, Z.; Mikhonin, A. V.; Asher, S. A. *J. Phys. Chem. B* **2007**, *111* (26), 7675–7680.
(40) Marqusee, S.; Robbins, V. H.; Baldwin, R. L. *Proc. Natl. Acad. Sci. U. S. A.* **1989**, *86* (14), 5286–5290.
(41) Merutka, G.; Shalongo, W.; Stellwagen, E. *Biochemistry* **1991**, *30* (17), 4245–4248.
(42) Cheng, R., P.; Girinath, P.; Ahmad, R. *Biochemistry* **2007**, *46* (37), 10528–10537.
(43) Lyu, P. C. C.; Gans, P. J.; Kallenbach, N. R. *J. Mol. Biol.* **1992**, *223* (1), 343–350.
(44) Bykov, S.; Lednev, I.; Ianoul, A.; Mikhonin, A.; Munro, C.; Asher, S. A. *Appl. Spectrosc.* **2005**, *59* (12), 1541–1552.
(45) Kallenbach, N. R.; Lyu, P.; Zhou, H. CD Spectroscopy and the Helix-Coil Transition in Peptides and Polypeptides. In *Circular Dichroism and the Conformational Analysis of Biomolecules*; Fasman, G. D., Ed.; Plenum Press: New York, 1996.
(46) Zimm, B. H.; Bragg, J. K. *J. Chem. Phys.* **1959**, *31* (2), 526–535.
(47) Cantor, C. R.; Schimmel, P. R. *Biophysical chemistry*; W. H. Freeman and Company: New York, 1980; Vol. III.
(48) Scholtz, J. M.; Qian, H.; York, E. J.; Stewart, J. M.; Baldwin, R. L. *Biopolymers* **1991**, *31* (13), 1463–1470.
(49) Yang, J. X.; Zhao, K.; Gong, Y. X.; Vologodskii, A.; Kallenbach, N. R. *J. Am. Chem. Soc.* **1998**, *120* (41), 10646–10652.
(50) Scheraga, H. A. *Pure Appl. Chem.* **1973**, *36* (1−2), 1.
(51) Wojcik, J.; Altmann, K. H.; Scheraga, H. A. *Biopolymers* **1990**, *30* (1−2), 121–134.
(52) Padmanabhan, S.; York, E. J.; Gera, L.; Stewart, J. M.; Baldwin, R. L. *Biochemistry* **1994**, *33* (28), 8604–8609.
(53) Zimm, B. H.; Doty, P.; Iso, K. *Proc. Nat. Acad. Sci. U. S. A.* **1959**, *45* (11), 1601–1607.
(54) Ostroy, S. E.; Lotan, N.; Ingwall, R. T.; Scheraga, H. A. *Biopolymers* **1970**, *9* (7), 749–764.

(55) Ptitsyn, O. B. *Pure Appl. Chem.* **1972**, *31* (1−2), 227.
(56) Daggett, V.; Kollman, P. A.; Kuntz, I. D. *Biopolymers* **1991**, *31* (9), 1115–1134.
(57) Wang, Y.; Purrello, R.; Jordan, T.; Spiro, T. G. *J. Am. Chem. Soc.* **1991**, *113* (17), 6359–6368.
(58) Woody, R. W.; Tinoco, I., Jr. *J. Chem. Phys.* **1967**, *46* (12), 4927–4945.
(59) Madison, V.; Schellman, J. *Biopolymers* **1972**, *11* (5), 1041–1076.
(60) Woody, R. W. Theory of Circular Dichroism of Proteins. In *Circular Dichroism and the Conformational Analysis of Biomolecules*; Fasman, G. D., Ed.; Plenum Press: New York, 1996.
(61) Ozdemir, A.; Lednev, I. K.; Asher, S. A. *Biochemistry* **2002**, *41* (6), 1893–1896.
(62) Mix, G.; Schweitzer-Stenner, R.; Asher, S. A. *J. Am. Chem. Soc.* **2000**, *122* (37), 9028–9029.
(63) Myshakina, N. S.; Asher, S. A. *J. Phys. Chem. B* **2007**, *111* (16), 4271–4279.
(64) Tinoco, I., Jr.; Halpern, A.; Simpson, W. T. The relation between conformation and light absorption in polypeptides and proteins. In *Polyamino Acides, Polypeptides, and Proteins*; Stahmann, M. A., Ed.; University of Wisconsin Press: Madison, 1961.
(65) Woody, R. W.; Koslowski, A. *Biophys. Chem.* **2002**, *101*, 535–551.
(66) Nymeyer, H.; Garcia, A. E. *Proc. Natl. Acad. Sci. U. S. A.* **2003**, *100* (24), 13934–13939.
(67) Zhang, W.; Lei, H. X.; Chowdhury, S.; Duan, Y. *J. Phys. Chem. B* **2004**, *108* (22), 7479–7489.
(68) Chakrabartty, A.; Kortemme, T.; Baldwin, R. L. *Protein Sci.* **1994**, *3* (5), 843–852.
(69) O'Neil, K. T.; DeGrado, W. F. *Science* **1990**, *250* (4981), 646–651.